World Electric Vehicle Journal

MDPI

Article

Hardware Implementation of a Resilient Energy Management System for Networked Microgrids

Hossam M. Hussein, S M Sajjad Hossain Rafin, Mahmoud S. Abdelrahman and Osama A. Mohammed *

Energy System Research Laboratory, Department of Electrical and Computer Engineering, Florida International University, Miami, FL 33174, USA; hhuss013@fiu.edu (H.M.H.); srafi010@fiu.edu (S.M.S.H.R.); mabde046@fiu.edu (M.S.A.)

* Correspondence: mohammed@fiu.edu

Abstract: A networked microgrid is composed of multiple nearby microgrids linked together to gain additional flexibility for resilient operations. Networked microgrids collaborate to prevent power shortages in microgrid clusters by sharing critical renewable and energy storage resources. However, controlling the local resources of each microgrid, including the energy storage systems' charging and discharging, maintaining the DC bus voltage, and even overseeing the power shared by multiple microgrids, is challenging. Therefore, a microgrid control technique and distributed energy management are used cooperatively in this study to handle the shared power between a system of networked microgrids incorporating photovoltaics and battery energy storage systems. Numerical simulation results from a networked microgrid system verify the accuracy and soundness of the suggested distributed energy management under several operating conditions, including renewable uncertainties and sequential load variations in different zones. The applicability of the suggested technique is confirmed by hardware implementation, and several operational scenarios further evaluate the proposed system on a practical two-microgrid system located in the Florida International University (FIU) testbed.

Keywords: microgrids; networked microgrids; renewable energy systems; energy storage systems; testbed; hardware-in-the-loop

Citation: Hussein, H.M.; Rafin, S.M.S.H.; Abdelrahman, M.S.; Mohammed, O.A. Hardware Implementation of a Resilient Energy Management System for Networked Microgrids. *World Electr. Veh. J.* **2024**, *15*, 209. https://doi.org/10.3390/wevj15050209

Academic Editors: Wenming Yang and Anna Pinnarelli

Received: 15 April 2024
Revised: 1 May 2024
Accepted: 6 May 2024
Published: 10 May 2024

1. Introduction

DC systems have attracted the utility operator's attention for their remarkable features in generation and distribution systems. In contrast to AC systems, DC microgrids have lesser power loss despite supplying around 1.4 times more than the equivalent AC microgrid configuration, according to the skin effect phenomena [1]. Additionally, the unidirectional power flow facilitates its control. Moreover, many technical concerns regarding the harmonics and power factor correction are absent. Furthermore, DC voltage can solely be used to indicate the system stability and state [2,3]. In the same context, conventional energy systems are witnessing a dramatic change due to the broad penetration of renewable energy resources (RESs) such as wind turbines and photovoltaic PV systems. These aggregated resources form what are known as microgrids (MGs). Despite that, the intermittent nature of these resources necessitates the existence of energy storage systems (ESSs) [4–6]. All these aspects result in the idea of DC MGs. However, several challenges come to the surface with this integration. The low inertia of these inverter-based resources results in a lack of stability in certain operating conditions, such as severe load patterns or constant power loads [7,8]. Further, the imbalance between load demand and generated power might lead to generation curtailment or load-shedding, which requires additional energy management systems with load and generation forecasting features to deal with such conditions [9–11]. The interconnection between these microgrids is a promising solution to these challenges [12,13].

The primary goals of networked microgrids (NMGs) revolve around enhancing system capabilities by harnessing distributed power sources [14], as well as bolstering system stability and reliability [15], maintaining an optimal state of charge (SoC) for ESS [16], optimizing the operational cost [17], and fortifying network resilience against unforeseen events by fostering synchronization between aggregated resources and load requirements [18,19]. Nonetheless, handling the local resources within each single microgrid with the uncertainty of the RES, the charging and discharging process of their ESSs, stabilizing the DC bus voltage, and managing the power shared between several MGs are considered challenging. With such massive systems, data must be collected and analyzed, and feedback signals are generated through the appropriate energy management system for specific actions [20]. These aspects can be handled by adding a communication layer to facilitate the data transfer.

Other major technical challenges stand against the wide spread of NMG systems. For instance, in microgrids, power flow occurs in multiple directions, posing challenges to conventional protection methods designed for unidirectional power flow systems. These fault currents fluctuations can adversely impact the protection system's fundamental aspects, including sensitivity, selectivity, reliability, and response speed. Moreover, various layers of protection must be explored within a multi-microgrid system, including converter- and circuit-breaker-based safeguards [21]. Furthermore, ensuring the effectiveness of protection measures across various operational scenarios, including radial and mesh configurations and grid-connected and islanded modes of microgrids, is essential. Consequently, several protection challenges arise, such as protection system impairment, loss of grid synchronization, erroneous tripping, and delayed tripping [22,23].

Additionally, the integration of Distributed Energy Resources (DERs) and the associated uncertainties pose potential risks to the overall stability of the systemassociated uncertainties pose potential risks to system if not properly accounted for. It is imperative to ensure precise management of voltage and frequency regulation [24]. Developing robust control strategies leveraging the rapid response capabilities of power electronic resources can effectively address these challenges [25,26]. Leveraging communication infrastructure enables coordination among various digital protection relays, offering solutions for numerous networked microgrid (NMG) systems. However, integrating information and communication technology introduces vulnerabilities, increasing the system's susceptibility to cyberattacks. Therefore, detecting and mitigating these threats is essential for maintaining overall system stability [27,28]. Hence, an efficient energy management system is crucial to manipulate all the data collected from these distributed systems and ensure efficient power flow among them [29].

Several energy management approaches were introduced to address these aspects. Their main objectives were to minimize the operational cost, reduce the computational burdens, enhance the system resiliency, and improve the communication flow. For instance, centralized, decentralized, distributed, and hierarchical energy management systems are the four main classical architectures in this regard [30,31]. The centralized approach collects information from various points in the system and manipulates these measurements through a centralized processing unit to perform optimal scheduling, power sharing, and stability enhancement. Any modifications to the local controllers or system parameters are managed through the centralized EMS. This process can be done through direct connection to these aggregated resources in small-scale systems or through proper communication networks for larger systems. The significant drawbacks of centralized architecture are the single point of failure and the substantial computational burdens and communication infrastructure when the network size becomes tremendous [32].

Decentralized EMSs were introduced to cope with these issues. In this architecture, each distributed resource receives its signal from its local controller to optimize its performance without further connection to the neighboring networks. Under this category, droop and model predictive control methods are the widely used control techniques to manage the shared power between the scattered resources and optimize the system performance [33].

However, this management topology is poorly performed without a communication layer between the adjacent networks. To cover this gap, distributed EMSs were presented. This architecture splits the system into two different zones: the device or local controllers' level, where each distributed resource receives its control signals from its local controller for voltage and current regulations, and the system or upper level that optimizes the shared power increases the system resiliency and smoothens the integration or disconnection of any MG [34].

The hierarchical EMS is more appropriate if the networked MG system becomes more complicated. Through three control layers, named primary, secondary, and tertiary, this energy management structure can significantly enhance the overall system performance. For the device level, the primary control with its fastest control action controls the power converters in each device to regulate the system current and voltage signals while suppressing any disturbance or transients. The secondary controller focuses mainly on synchronizing the operation between the networked MGs or grid connection for the grid-connected mode. The control action speed at this level is slower than that at the primary level for day-ahead load forecasting and operation cost optimization. This hierarchical architecture provides a swift and smooth transition between the operating states [30,33,35].

Different control techniques were used within each layer of the previously mentioned EMSs. As each layer has a specific task and a certain amount of data to manage, the complexity of the control techniques varies from one layer to another. For instance, through the device level, PID controllers are widely used where they can provide sufficient performance [36]. Additionally, intelligent controllers based on fuzzy logic and neural networks are applicable at this level [37]. The control techniques became more complex as we went to the upper levels. Adaptive droop controllers were used at the system level to balance the shared power among the distributed resources while maintaining the system stability [38].

Moreover, model predictive controllers (MPCs) are considered one of the most efficient tools for EMSs that can be utilized through any of the three mentioned layers [39]. With scattered resources, such as in the NMGs, the distinct features of multi-agent systems (MAS), such as communication, coordination, and autonomy, are utilized to achieve bidirectional information and energy interaction [40]. With the aid of algorithms such as graph theory [41], particle swarm optimization [42], and genetic algorithms [43], the MAS control strategy can provide remarkable performance in NMGs. The consensus algorithm is also considered a promising approach in NMGs management systems [31].

Selecting the proper management system is mainly based on the system architecture, the system's size, and the type of loads [44]. For instance, when the system includes many MGs, the amount of data to be manipulated will become huge. Further, the existence of the communication layer will be vital to precisely measure the system status and allow faster control of the feedback action in reverse. However, concerns regarding system security and data fidelity will surface. For instance, man-in-the-middle (MIM), denial-of-service (DoS), and false data injection (FDI) are kinds of cyber-attacks through communication networks. These cyber threats will necessitate further security and authentication layers, complicating the EMS structure and delaying the needed command action. In this regard, balancing the system requirements regarding the number of measured data and the needed control actions for the capabilities and data security provided by the appropriate EMS system is imperative [30,45–48].

NMG is widely utilized in many applications, such as shipboard power systems, electric aircraft, military bases, and electric vehicles, as well as the expected transition of the traditional utility grid to the same concept in the coming years. The existence of such hardware testbeds for experimental consideration is crucial for scientific researchers. In this essence, testing and validating the proposed control techniques and the EMSs is well supported with hardware verification. In this regard, the main contribution of this work is to provide a detailed hardware implementation of the NMG system at the energy systems research laboratory (ESRL). The focus of this research can be summarized as follows:

- Providing a detailed hardware implementation of a system of two interconnected microgrids at the ESRL smart-grid testbed.
- Experimental validation of the proposed control technique for MG during uncertainties in PV generation.
- Develop and verify the hardware implementation of a distributed energy management system to handle the shared power between the NMG systems under different loading conditions.

The rest of this paper is organized in the following way: Section 2 provides the modeling and architecture of the proposed model. Section 3 covers the proposed EMS and the simulation results, while Section 4 explains the hardware and experimental configuration. The experimental results and analysis are in Section 5, with the conclusion in Section 6.

2. System Architecture and Modelling

The construction of NMGs and the specifics of microgrid components are all explained in this section. A simple diagram of the complete system is shown in Figure 1. This proposed system has been designed and implemented in the FIU testbed. As shown in Figure 1, the system under investigation consists of two DC microgrids providing various load profiles and connected with a common DC bus through controlled circuit breakers (CB1 and CB2). Two local MG controllers control and manage the associated MG operations by adjusting the output of connected resources based on the load requirements. In addition, there is an energy management system on the top layer (EMS) to monitor and manage the power and energy contribution of each MG to supply a common DC bus load as well as power exchange between the two MGs.

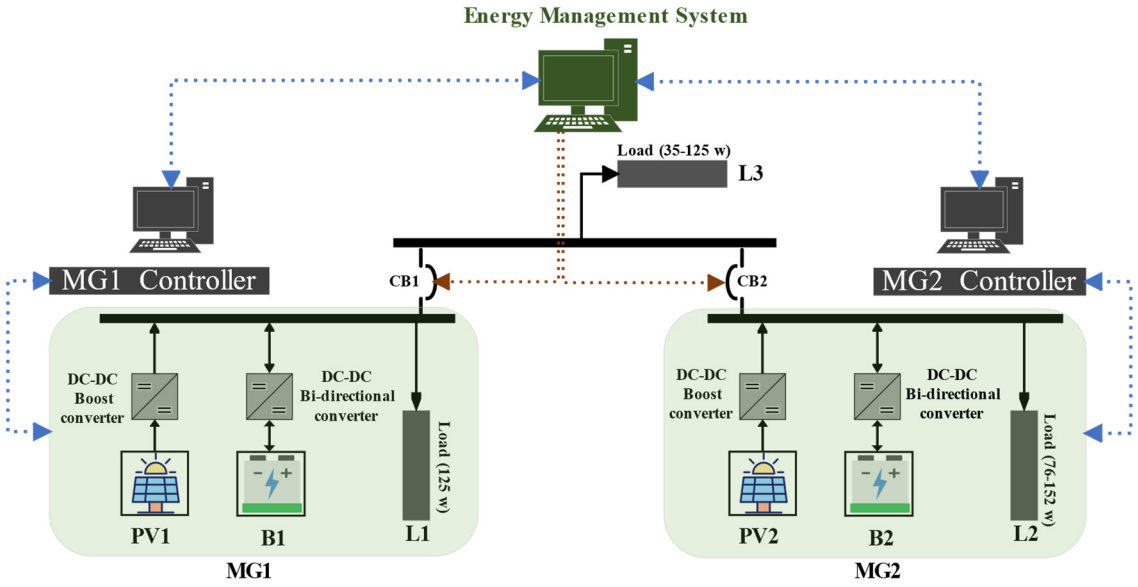

Figure 1. Networked microgrid architecture in this study.

2.1. PV System Model

Looking at the structure of each microgrid, as depicted in Figure 2, more details will emerge. The MG includes a PV module connected to the DC bus through a DC/DC boost converter, as shown on the left side. The local controller of the MG switches between the conventional PI or MPPT controlling mode according to the available generation and total load requirements through the NMGs. Other rules might be settled during the experimental validation to minimize the system variations and enhance the EMS performance. There are several methods for modeling a solar PV array. This work uses a five-parameter model to simulate the PV array [49]. It uses a current source powered by sunlight in parallel with a series resistor, a shunt resistor, and a diode connected to the output.

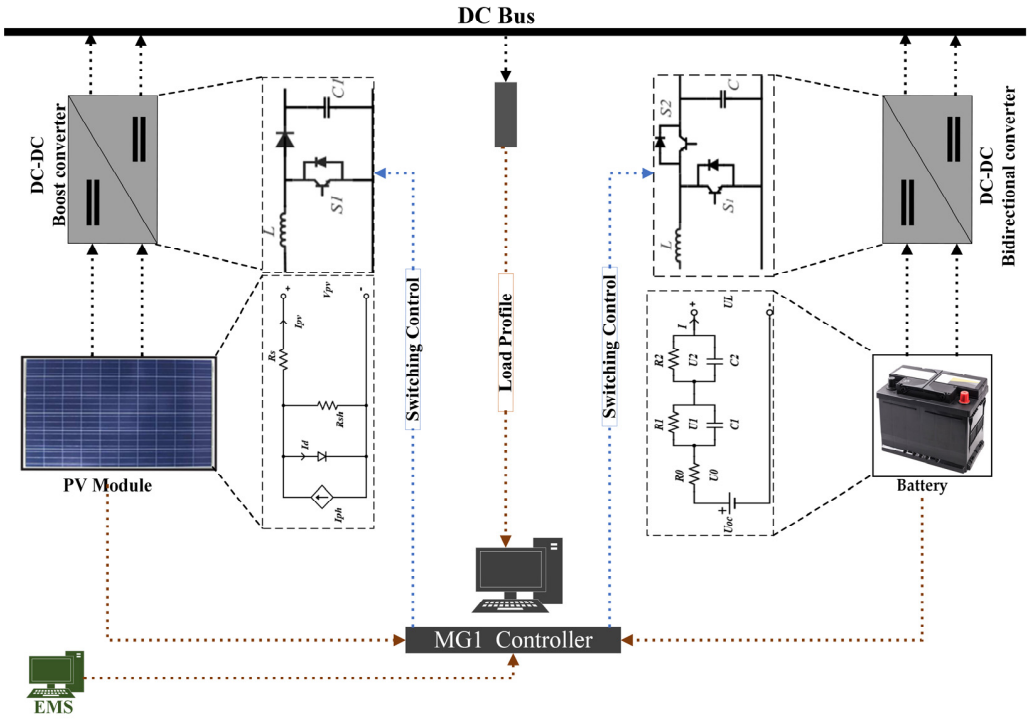

Figure 2. Detailed architecture of each MG.

The PV-generated output power depends on various factors, including solar radiation, weather conditions, and module efficiency. To conceptualize a simplified model of any PV system, essential information such as module open circuit voltage, short circuit current, and maximum power point must be considered. If additional details are accessible, a more comprehensive practical model, as depicted in Figure 2, can be furnished. This model can be articulated mathematically, as demonstrated in Equation (1):

$$I_{pv} = I_{ph} - I_o \left[exp \left(\frac{V_{pv} + I_{pv} R_s}{a \frac{kT}{q}} \right) - 1 \right] - \frac{V_{pv} + I_{pv} R_s}{R_{sh}} \quad (1)$$

where V_{pv} is the terminal voltage, the photocurrent is represented as I_{ph}, I_o the saturation current, the medium temperature is T, R_{sh} is the shunt resistance, while R_s is the series resistance. Further, a, q, and k are constants named as ideality factor, electron charge, and Boltzmann constant, respectively.

Among the available RESs, solar energy is more universally available than wind energy, with consistent access to sunlight in most regions. Furthermore, PV technology has advanced rapidly in recent years, with declining costs and increasing efficiency. Additionally, PV microgrids typically require less land area for installation than wind farms, making them more suitable for urban and residential applications. Further, it can be easily scaled up or down to fit energy needs. This scalability makes them suitable for research purposes, where experimentation with different sizes and configurations is often necessary, whereas in our case, for DC microgrids, the control techniques are simpler, no frequency regulation is needed, and the variable parameters are less.

2.2. Battery Energy Storage System (BES) Model

Microgrids are local electrical networks that include generation, storage, and essential loads that can function both in grid-connected and islanding scenarios. Therefore, energy storage systems like batteries are crucial to smooth this transition. However, in special types of MGs, such as the shipboard MG, to keep the system stable against any significant load fluctuation by dynamic loads such as propulsion motors and pulsed loads, a hybrid ESS consisting of battery and supercapacitor is used to manage these power changes

adequately [44]. Compared to lead-acid batteries, Li-ion batteries offer higher power and energy density capacities. They can also provide the load at a constant current because of their modest voltage variation while discharging [36].

Regarding the energy storage system in this study, lithium-ion batteries (LIBs) are used and attached to the DC bus through DC/DC bidirectional converters. This configuration will facilitate the battery charging/discharging when the PV generation is above/below the load requirements. The main objective of the ESS is to stabilize the DC bus voltage against any disturbances. Hence, the bus-voltage signal will be given to the battery controller to generate the proper action of charging or discharging the battery.

The Thevenin equivalent circuit model (ECM) is widely utilized to calculate the battery voltage in response to the current, as in Figure 2. According to [50], an ideal voltage source that is associated with the state of charge of the battery (SoC) represents the OCV. R_0 represents the battery's ohmic resistance, and the parallel RC network represents its transient behavior resulting from interfacial charge-transfer reactions at the electrode (R1 and C1). The Thevenin ECM is as follows:

$$V = OCV - R_O \cdot I - U_1 \tag{2}$$

where OCV represents the open circuit voltage, R_O is the internal resistance, I is the battery current, V is the battery terminal voltage, and U_1 is the voltage of the RC circuit. If a large SoC functioning range needs to be simulated, SoC can be considered as influencing the parameters, and the model is defined by (2):

$$V\ (SoC) = OCV(SoC) - R_O(SoC) \cdot I - U_1(SoC) \tag{3}$$

2.3. DC/DC Converter System Model

The DC/DC converters are employed in numerous applications where the energy supply is insufficient for the activity of such applications. In the microgrid, a buck or boost converter has been used to convert DC voltages to the rated DC voltage. The boost converter is a sort of DC/DC converter that has a yield voltage that is higher than the supplied input voltage. The buck converter modifies the voltage so that it is less than the input voltage that is being supplied. The buck–boost converter is one type of DC/DC converter that can provide an output voltage that is either higher or lower than the input voltage. Furthermore, a bidirectional buck–boost converter provides power stream reversal.

As stated earlier, two different DC/DC converters were used in this study, as shown in Figure 3. A boost converter with a PV system, as given in Figure 3a, and a bidirectional one for the ESS as shown in Figure 3b. In general, a unidirectional DC/DC converter can be made bidirectional by adding a governable switch to replace the diodes in the circuitry. However, multiple changes must also be considered regarding the operating conditions and the switching portions [51]. For instance, the boost converter inductance and capacitance must be selected accurately and at a level higher than the converter critical values to maintain system stability. To be specific, during the operation of the boost converters, the inductance must be sufficient to maintain the continuity of the inductor current.

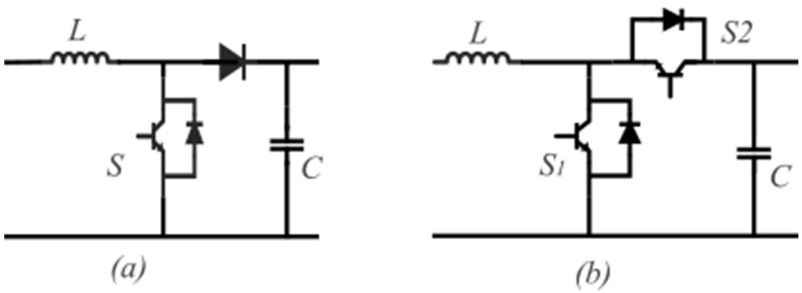

Figure 3. DC/DC converters: (**a**) boost; (**b**) bidirectional.

Similarly, for the capacitance to keep, the capacitor voltage exists. Additionally, minimizing the system ripple relies on these two values. These critical values can be obtained as follows [52]:

$$L_C = \frac{D(1-D)}{2f} R \tag{4}$$

$$C_C = \frac{D}{2fR} \tag{5}$$

where D is the duty cycle, the switching frequency is mentioned as f, and the load resistance is R. Since the switching frequency is normally kept constant during the operation, care should be considered with the worst load condition to achieve a precise design.

Further considerations must be included with the bidirectional converter as well. Normally, ESSs and batteries especially are known for their sophisticated dynamics. To handle this issue, filters are crucial to save the system operation and surpass converters' ripples and overshoots on both sides. As an illustration, the load has a lesser effect here in the filter's values. Selecting the proper filter limits relies more on the acceptable ripples through the system operation in the buck–boost converter's high and low voltage sides. The following equations can be used to determine the appropriate values of the L and C filters [52]:

$$\Delta I_{HV} = \frac{DV_{in}}{f\,L} \tag{6}$$

$$\Delta V_{HV} = \frac{DI_{out}}{f\,C} \tag{7}$$

$$\Delta I_{LV} = \frac{D\,(V_{in} - V_{out})V_{out}}{f\,L\,V_{in}} \tag{8}$$

$$\Delta V_{LV} = \frac{D\,(1-D)V_{in}}{8\,f^2\,L\,C} \tag{9}$$

where ΔI_{HV} and ΔV_{HV} are the targeting ripple current and voltage in the high voltage side, respectively, while ΔI_{LV} and ΔV_{LV} are the same for the low voltage side, the bidirectional input voltage is V_{in}, and its output voltage and current signals are denoted as V_{out} and I_{out}, respectively.

The bidirectional converter controls the DC voltage by controlling the duty cycle. This controller maintains a constant voltage at the yield side when operating in both boost and buck modes. The controller generates the duty cycle of both switches. A proportional-integral (PI) controller regulates the DC/DC converter to maintain the reference output voltage.

3. Proposed EMS and Simulation Results

Integrating renewable energy sources and energy storage systems into microgrids has become crucial for ensuring a reliable and sustainable power supply. The NMGs in this study are working under different operating conditions and variations. These variations occur in one of the microgrids, such as reducing the PV generation and increasing the load demand. Further, the typical common load (L_C) shared among the two microgrids is witnessing a load variation, including sequential decreasing or increasing to test the performance of the EMS. Through these variations, local controllers handle their local demands according to their local measurements. In the upper layer, the EMS monitors the status of each microgrid in terms of voltage and load condition, besides ensuring steady power sharing between the two MGs. The proposed EMS system is presented in Figure 4 followed by the proposed Algorithm 1. It is worth mentioning that each BES will charge during slight loading conditions and according to their associated PV generation capacity. Further, MG1 is considered a slack bus in this work.

Algorithm 1: Proposed energy management system (EMS) (upper level)

Initialize MGs controller and EMS parameters.
Read P_{MG1}, P_{MG2}, and L_C.
for i = 1
  Compute $\Delta P = P_{MG1} + P_{MG2} - P_{LC}$
    if $\Delta P > 0$ **"Minor"**
      charge batteries with lower PV generation.
    else if $\Delta P = 0$ **"critical"**
      discharge BES1 and BES2.
    else
      disconnect the common load.
end for

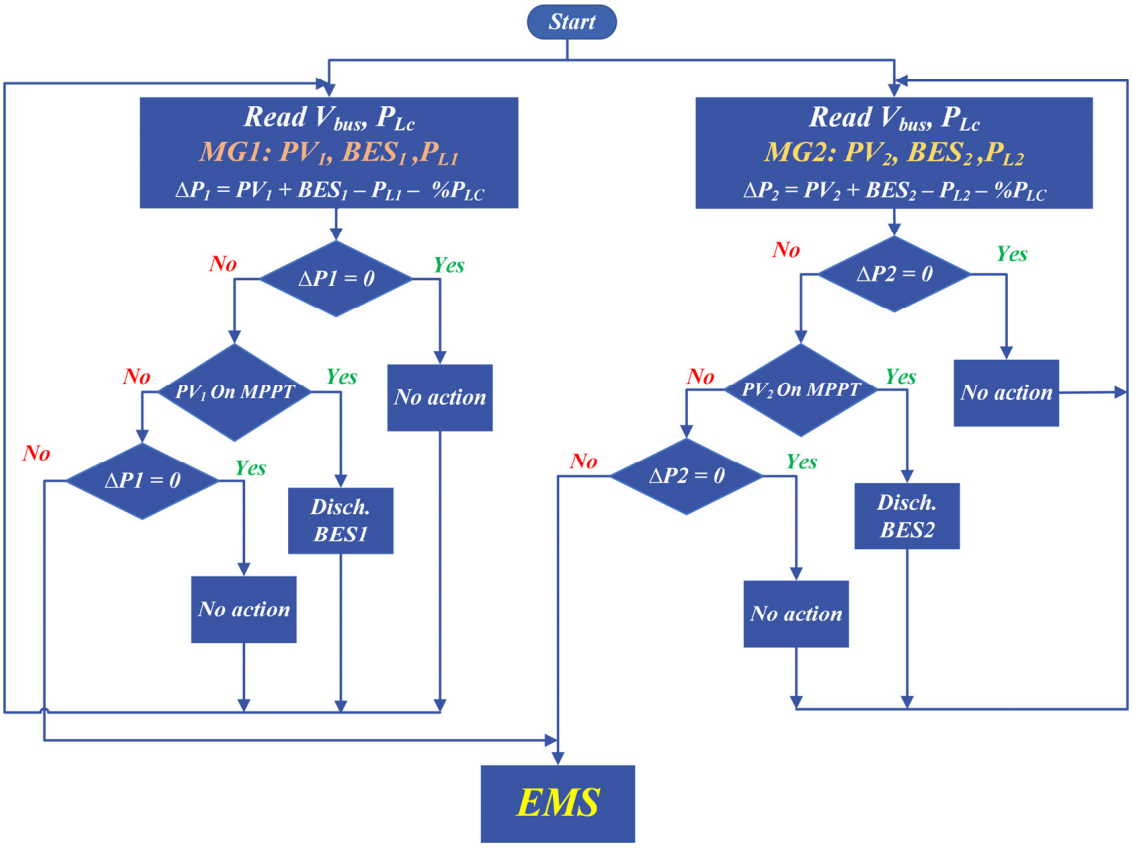

Figure 4. Proposed EMS for the hardware setup (lower level).

The designed EMSs were tested through the MATLAB/Simulink model with the same architecture, load, and generation profiles. The simulation results included two cases for the first operation scenario. This scenario explored the local controllers and the upper-level EMS's performance when the load demands go beyond the generation capabilities. As shown in Figure 5, the PV generation was reduced by about 40% in case a. Hence, the local storage system reacted immediately to fill this gap. This clearly appears in Figure 6, where the aggregated power did not change, and no power was shared between MG1 and MG2. However, in case b, the situation changed. We set a discharge limit to secure the BES in MG2. When the load in MG2 increased, the MG could not supply that request. Therefore, the EMS (upper level) acted in this case and provided the needed power from MG1, as shown in Figures 5 and 6 through case b.

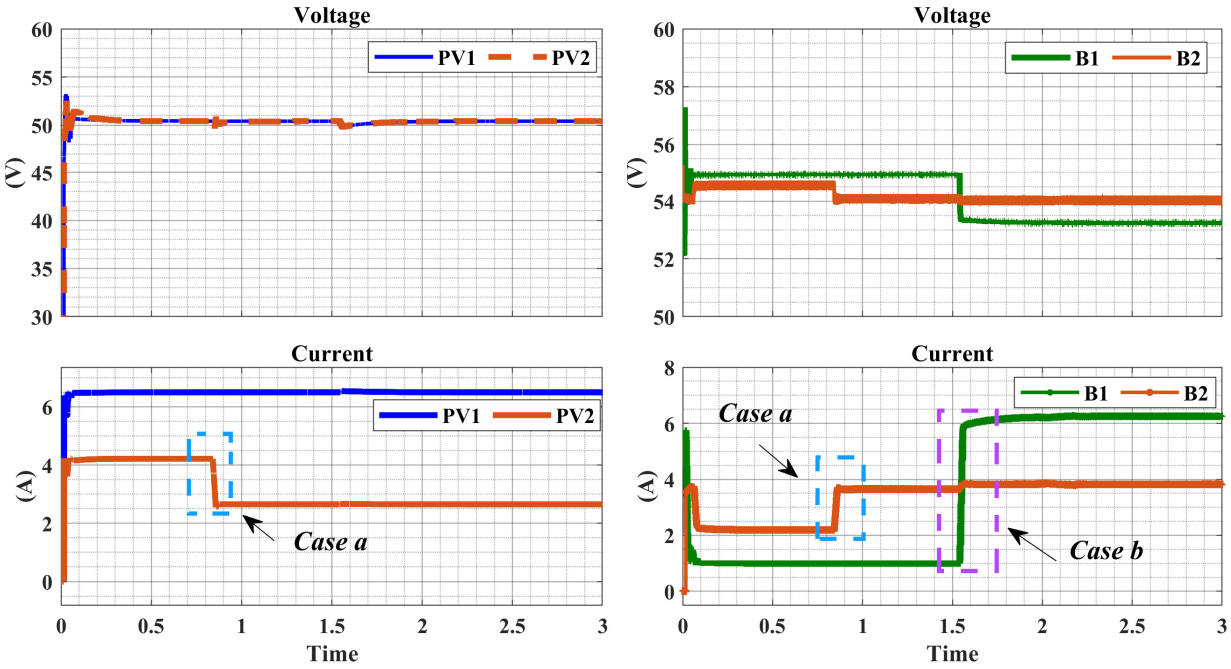

Figure 5. Simulation results of PV and Battery of each MG in scenario 1.

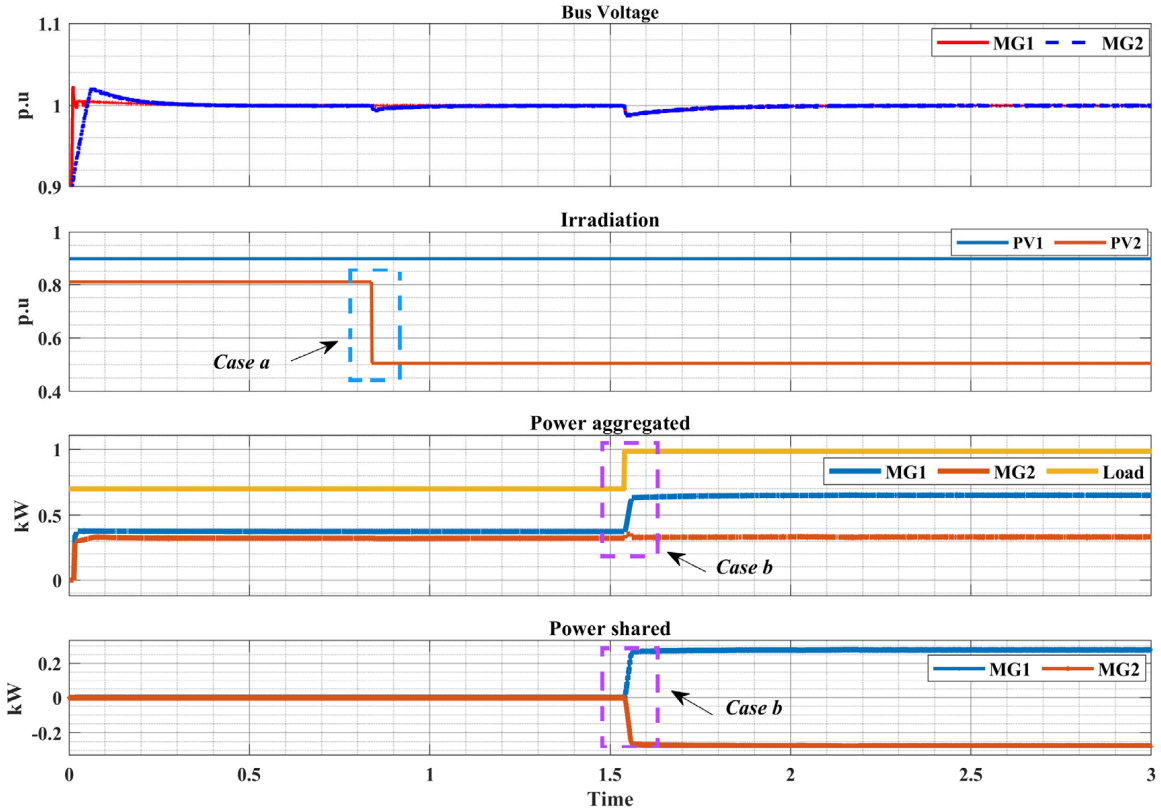

Figure 6. Simulation results of NMGs in scenario 1.

As the simulation results provide a promising performance for the proposed EMS, the following step is to implement the two-level EMS in the hardware testbed. The rest of this chapter will explore the power-sharing capabilities of an interconnected microgrid system consisting of two microgrids, MG_1 and MG_2, under various scenarios and cases. MG1 comprises a 350 W photovoltaic (PV) system (PV_1) acting as a current source, a 100 Ah

battery energy storage system (BES_1), and a 125 W local load (L_1). MG2 incorporates a 300 W PV system (PV_2) functioning as a current source, a 100 Ah battery energy storage system (BES_2), and a local load (L_2) ranging from 76 W to 152 W. A common load (L_C) ranging from 35 W to 125 W is situated between the two microgrids and can be supplied by either microgrid or both, depending on power availability and disturbances. The microgrids are interconnected, enabling them to supply power to each other's local loads in case of shortages or disturbances. MG_1 is designated the slack bus, with BES_1 acting as the swing generator, maintaining the DC bus voltage.

3.1. Scenario 1: Impact of Reduced PV Output and Load Variation on MG_2

3.1.1. Case 1: Effect of 60% Negative Irradiation Change on PV_2

This case investigates the effect of a 60% reduction in PV power output from MG_2 on the interconnected system. The focus is on how the batteries in both microgrids, BES_2 and BES_1, respond to the reduced PV output from PV_2.

3.1.2. Case 2: Increased Load on MG_2 with Reduced PV Output

Building upon Case 1, this case examines the impact of a 100% increase in the local load (L_2) of MG_2, while the PV power output remains reduced by 60%. This study demonstrates how the system copes with the drastic change in load demand with the decreased PV supply from MG_2. In both cases, the DC bus voltage, a local load of MG_1 (L_1), and the common load (L_C) remain unchanged.

3.2. Scenario 2: Power Sharing during Common Load Variations

3.2.1. Case 1: Common Load Variations with Unchanged PV Supplies

This case varies the common load (L_C) in two steps to observe the effect on power flow between the microgrids. Since the PV supplies remain unchanged due to constant irradiation, power sharing occurs primarily between the battery energy storage systems (BES_1 and BES_2).

3.2.2. Case 2: Common Load Variations with Reduced PV Output in MG_2

In this case, the common load (L_C) varies in four load steps, while the PV output of MG_2 (PV_2) is reduced by 50% due to a 50% reduction in irradiation. Additionally, the battery energy storage of MG_2 (BES_2) requires charging. This case studies the impact of these events and how the system mitigates the issues. In both cases, the DC bus voltage's local loads of MG_1 (L_1) and MG_2 (L_2) remain unchanged.

Table 1 provides a summary of the scenarios and cases for various changes within MG_1 and MG_2. Moreover, the table also includes the probable impact. The experiment and result analyses conducted in these scenarios and cases are described in detail in Sections 4 and 5 to demonstrate the power-sharing capabilities of the interconnected microgrid system under various operating conditions. The results highlight the system's ability to maintain power balance, manage fluctuations in renewable energy sources, and ensure reliable power supply to local and common loads. The findings provide valuable insights into the design, operation, and control of interconnected microgrid systems, contributing to advancing resilient and sustainable energy systems.

Table 1. Summary of the scenarios and cases.

Scenarios	Cases	MG	Solar PV (PV_1 and PV_2)	Local Load (L_1 and L_2)	Common Load (L_C)	BES DC Bus Voltage
Scenario 1	Case 1	MG_1	Change depending on PV_2	Unchanged	Unchanged	Unchanged Unchanged
		MG_2	60% reduction	Unchanged		Automatically changed to compensate for the PV_2 reduction.

Table 1. *Cont.*

Scenarios	Cases	MG	Solar PV (PV_1 and PV_2)	Local Load (L_1 and L_2)	Common Load (L_C)	BES DC Bus Voltage
Scenario 1	Case 2	MG_1	Unchanged	Unchanged	Unchanged	Automatically changed to compensate for the L_2 increase
		MG_2	60% reduction	100% increase		Unchanged
Scenario 2	Case 1	MG_1	Unchanged	Unchanged	Changes in 2 load steps	Automatically changed to compensate for the L_C variation
		MG_2	Unchanged	Unchanged		Automatically changed to compensate for the L_C variation
	Case 2	MG_1	Unchanged	Unchanged	Changes in 4 load steps	Automatically changed to compensate for the PV_2 and L_C variation
		MG_2	50% reduction	Unchanged		Requires charging

4. Hardware and Experimental Configuration

Creating an ideal control and monitoring architecture is one of the problems involved with microgrid implementation. The necessity to develop various testbeds that replicate the behavior of physical systems in real-time, along with the ongoing advancements in computer systems, has resulted in the usage of sophisticated, costly, and intricate simulation tools. The drawback of conventional simulation systems is that they cannot replicate the real-world operational environments of physical systems. Using the hardware-in-the-loop (HIL) real-time simulation (RTS) technique, which closes the simulation-to-real-world gap, is a suggested way to tackle this issue [53]. However, these testbeds primarily depended on software simulations rather than full hardware implementation. Hence, there is a lack of accurate and practical results. In essence, the absence of testing platforms where theories, practical restrictions, and simulation results may be reliably confirmed is a major driver for developing and implementing fully hardware testbeds. In this work, to verify the effectiveness of the energy management strategy and the control analysis of the proposed system, a hardware implementation is established in the testbed, as shown in Figure 7. The following subsections demonstrate a fully adjustable and controllable networked DC microgrid testbed designed and implemented at FIU. Each microgrid consists of renewable energy resources, energy storage systems, and controllable loads and can operate as a standalone microgrid or cooperatively with other microgrids.

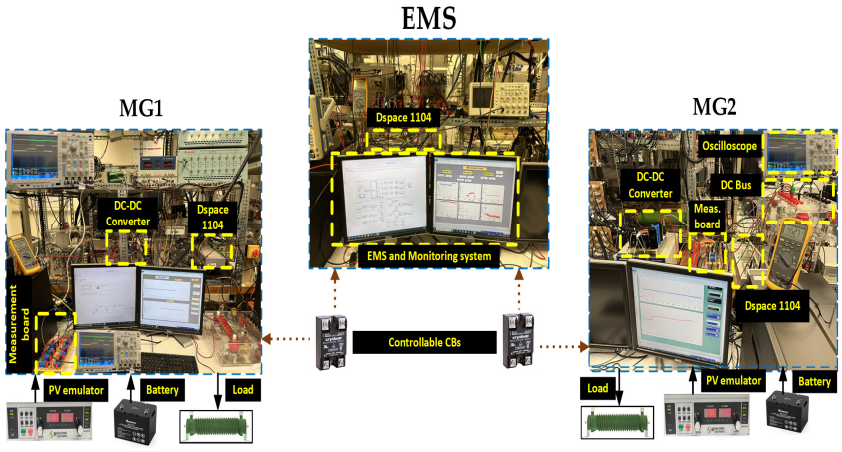

Figure 7. Hardware implementation of NMGs.

4.1. PV Emulator and Battery

Solar power generation is highly dependent on the external environment, making it challenging to construct an experimental environment utilizing actual PV panels. Therefore,

PV emulators can simulate how a real PV system would operate in different environmental scenarios [54,55]. Furthermore, the emulator may easily be coupled with the DC/DC converter and build an I-V curve using variations of load and daylight. It allows a variety of I-V and P-V curves for different solar radiation values to be simulated in the testbed regardless of actual solar radiation levels. The emulator can also simulate abrupt, quick variations in voltage so that you may see how the system and its parts behave under extreme circumstances. In this work, two 6 kW Magna-Power (Model: XR600-9.9/2008+HS) programmable power supplies can be set up to follow a predetermined power–time curve or to mimic solar characteristics. Figure 8a shows the P-V and P-I curves, and the resulting voltage and current with time are shown in Figure 8b.

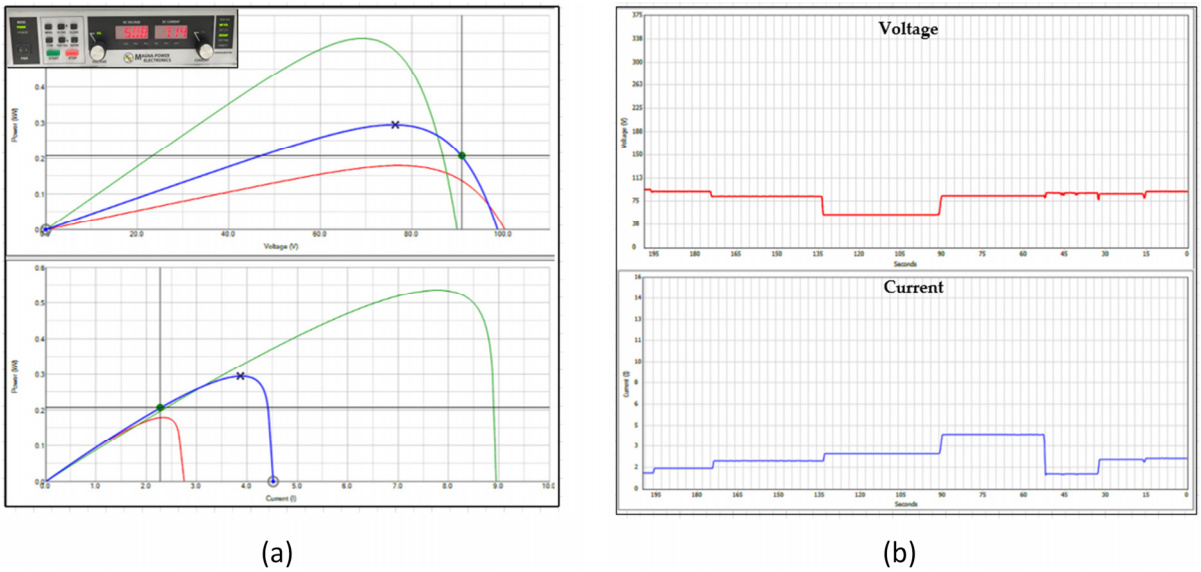

Figure 8. PV emulator output curves: (**a**) V/P and I/P curves at different irradiance conditions; (**b**) voltage and current outputs versus time.

4.2. Battery System

Energy storage devices such as batteries are required for a high energy penetration rate into a power system due to the intermittent nature of renewable energy. When the power system has an abundance of electricity, battery storage absorbs it and returns the excess back to it when it is most needed. Lead-acid and Li-ion technologies show promise for PV-integrated residential microgrids [56]. Lithium-ion batteries outperform lead-acid at a marginally higher cost in all critical performance criteria, such as round-trip efficiency and cycling capacity [57]. Lithium-ion batteries are the most widely utilized battery type in the commercial sector because of their many advantages, including high energy density, little memory effect, and rapid charge and discharge rates. This work uses 12 V, 100 Ah Smart lithium-ion batteries ($LiFePO_4$) in the two microgrids. Its parameters are given in Table 2.

Table 2. Parameters of batteries.

Parameter Description	Value
Rated capacity	100 Ah
Nominal voltage	12 V
Charging voltage	14.4 V
Max. continuous charging current	50 A
Discharging voltage range	10~14 V
Max. continuous charging current	100 A

4.3. DC/DC Converters and Controllers

The DC/DC bidirectional converter configuration and its PCB-based hardware test setup are shown in Figure 9. The same circuit board was utilized as a boost converter in our system. A separate diode board was connected to the output of the boost converter to prevent the current from passing in the reverse direction, besides controlling that through the control design. Table 3 shows the parameters of the converters.

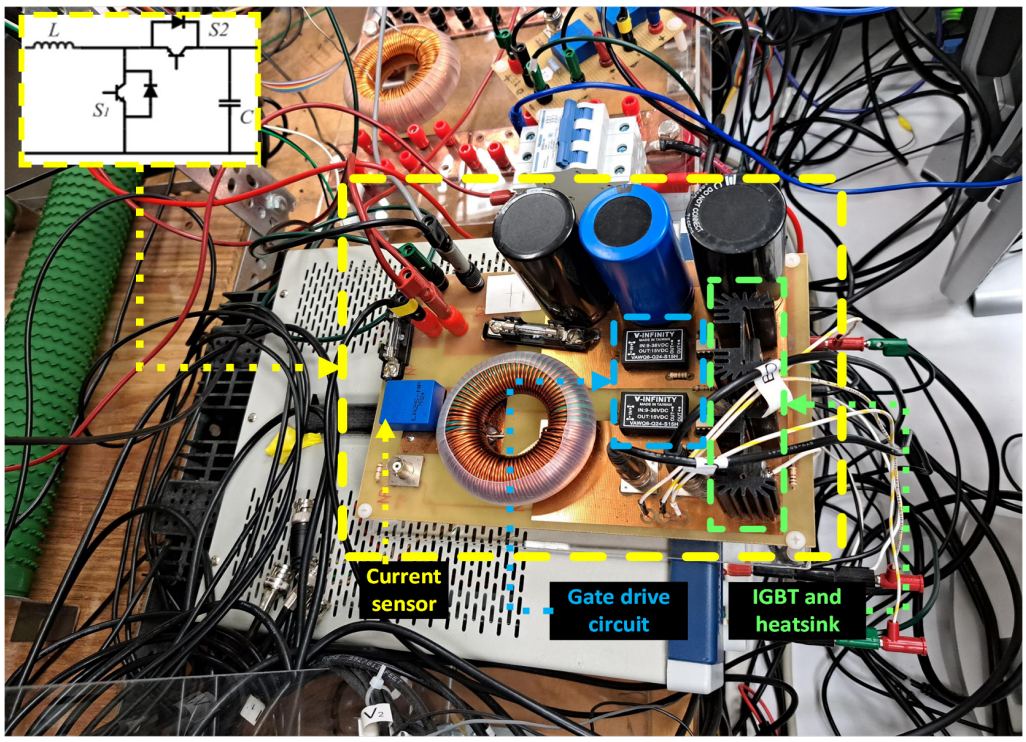

Figure 9. DC/DC bidirectional configuration and circuit board.

Table 3. DC/DC Bidirectional converter parameters.

Parameter	Description	Value
P	Power rating	2 kW
Vdc	High-side voltage	160 V
Vb	Low-side voltage	12 V
L	Filter inductor	3 mH
C	Filter capacitor	1200 µF
Fs	Switching frequency	5 kHz

4.3.1. Real-Time Control and Monitoring

The dSPACE 1104 real-time control module carries out the control of the power converters in each DC microgrid. As shown in Figure 10, the dSPACE 1104 board is utilized to control the DC/DC boost converter and bidirectional converter implemented in each microgrid. The dSPACE 1104 real-time interface controls the microgrid operation through the converter switching control, which was designed using the Matlab/Simulink R2022a software platform. Moreover, this control board is utilized for monitoring the energy management systems when both MGs are connected to the common DC bus system. The voltage and current are sensed through custom-designed metering systems utilizing the voltage transducer LV2S-P and the current transducer LA2S-NP by LEM.

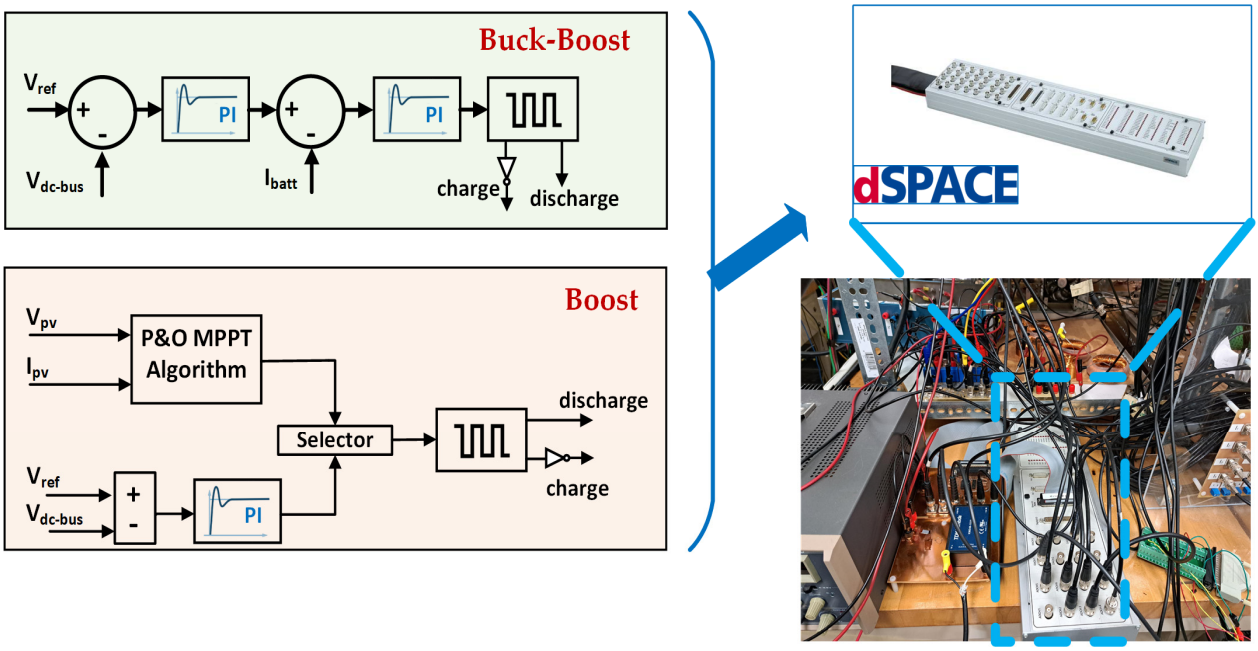

Figure 10. Controllers for each DC/DC converter implementation on the dSPACE platform.

4.3.2. Bidirectional Converter Control

A bidirectional DC/DC interface is necessary for battery storage devices to regulate their charging and discharging procedures. The developed converter can operate between the DC bus and battery voltage. To obtain the intended reference current signal in both the charging and discharging phases, two PI controllers were used with different K_p and K_i, as listed in Table 4. Figure 10 shows the controller implementation on dSPACE 1104.

Table 4. DC/DC converter controller parameters.

Parameter	Description	Value
	Bidirectional converter controller	
K_p	Proportional gain (voltage/current controllers)	0.002/0.02
K_i	Integral gain (voltage/current controllers)	110/3
	Boost converter controller	
K_p	Proportional gain	0.002
K_i	Integral gain	0.2

4.4. Load Emulation

Many loads use DC power, such as household products like computers, phones, microwave ovens, and lighting. Connecting loads via easier and more effective power-electronic interfaces is one of the main benefits of a DC microgrid. Energy management and power control are important issues for DC-powered loads, especially when different load profiles are required during the operation. To test the control and management effectively and accurately for a specific load profile, using fixed loads with manual connections is not enough, and load emulation must be used. This work includes two kinds of loads in the DC microgrid implementation: steady-state loads and dynamic loads. The rated power of the steady-state load is 2 kW at the rated DC bus voltage. The dynamic load is built using a 100 Ω resistor that is connected to a switching board controlled by a control algorithm on the dSPACE. As shown in Figure 11, the required load profile is sent to the controller to produce a specific switching pattern, resulting in the desired dynamic load behavior

during the test. This load emulator can fully emulate the dynamic behavior of a load up to 6 kW and the pulsed load effects.

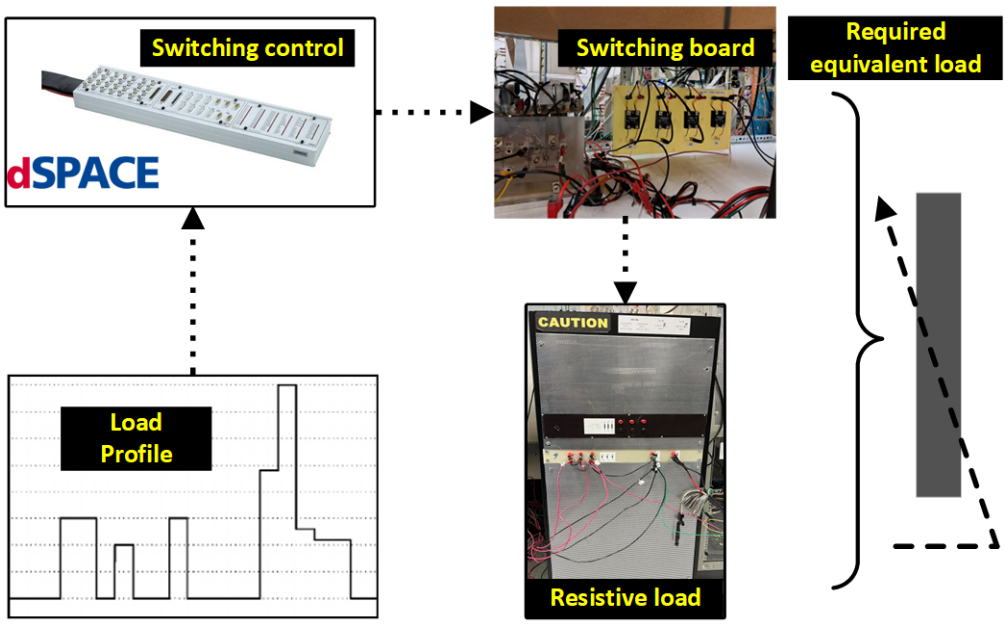

Figure 11. Programmable variable load and its control circuit board.

5. Experimental Results and Analysis

As described in the previous section, MG_1 comprises a 600 W photovoltaic (PV) system (PV_1) acting as a current source, a 100 Ah battery energy storage system (BES_1), and a 125 W local load (L_1). MG_2 incorporates a 500 W PV system (PV_2) functioning as a current source, a 100 Ah battery energy storage system (BES_2), and a local load (L_2) ranging from 76 W to 152 W. A common load (L_C) ranging from 35 W to 125 W is situated between the two microgrids and can be supplied by either microgrid or both, depending on power availability and disturbances. The microgrids are interconnected, enabling them to supply power to each other's local loads in case of shortages or disturbances. MG_1 is designated as the slack bus, with BES_1 acting as the swing generator, maintaining the DC bus voltage. Table 5 presents the specifications of the interconnected microgrid system.

Table 5. Specification of the interconnected microgrid.

Microgrid	Types of Energy Generation	Bus Voltage (V)	Power Rating (W) or Battery Capacity (Ah)	Local Load Range, L_1, and L_2 (W)	Common Load, LC (W)
MG_1	PV_1	50	350 W	125	35–125
	BES_1		12 V/100 Ah		
MG_2	PV_2		300 W	76–152	
	BES_2		12 V/100 Ah		

5.1. Scenario 1: Impact of Reduced PV Output and Load Variation on MG_2

5.1.1. Case 1: Effect of 60% Negative Irradiation Change on PV_2

Initially, PV_2 and BES_2 supplied L_2 of 76 W with a constant DC bus voltage of 50 V. The values of L_1 and L_C are 125 W and 42 W, respectively, and they remain unchanged for Case 1 and Case 2 of Scenario 1. Currently, the currents supplied from PV_2 and BES_2 are 1.5 A. After a certain period, due to a 60% reduction in solar irradiation, the PV_2 output current becomes 0.57 A, approximately 60% less than the initial condition. To compensate for the current requirement to run the 76 W local load, BES_2 generates more current, supplying

3 A (the maximum amount of current BES_2 can generate). This case and its results indicate that MG_2 is designed such that its power generators can handle power within their range if one fails within a specific range. Moreover, this interruption does not affect the operation of MG_1 and the local load service. In all cases, the BES' currents are measured from the battery side, not the DC bus side.

5.1.2. Case 2: Increased Load on MG_2 with Reduced PV Output

Continuing from Case 1, when BES_2 reached its maximum limit, a rapid load increment occurred, doubling the Case 1 value to 152 W. In this instance, PV_2 and BES_2 of MG_2 could not supply adequate power to L_1, L_2, and/or L_C demand. Consequently, BES_1 of MG_1 started to share power with L_2 and L_C by delivering 3.1 A, when at the initial condition, it delivered 1.5 A. Moreover, the supply from BES_2 and PV_2 remained unchanged. During power sharing in such conditions, BESs are used to share power for fluctuating or rapid load demand, as PV sources (current source elements) are irradiation-dependent for energy generation. This case demonstrated the ability of the interconnected microgrids to share power from one microgrid to another within their limits. Table 6 summarizes these two cases with their respective results.

Table 6. Summary of Scenario 1 and respective experimental results.

Scenario and Cases		Scenario 01	
		Case 01	Case 02
Load Profile (W)	L_1	125	125
	L_2	76	152
	L_C	42	42
Total Load (W)	L_T	243	319
PV_1 Current (A)		1.56 / 2.25	2.25
BES_1 Current (A)		1.50 / 1.50	3.42
PV_2 Current (A)		1.50 / 0.57	0.57
BES_2 Current (A)		1.50 / 3.00	3.00

Figure 12a–c illustrate the behavior of Scenario 1, which comprises Case 1, where a reduction in the output from PV_2 prompts BES_2 to compensate by increasing its power supply, thereby ensuring the load demand is met, and Case 2 where an escalation in the load demand of L_2 necessitates the intervention of BES_1 from MG_1, which steps in to supplement the power supply and meet the increased load requirements. It is to be noted that Figure 12a shows the experimental measurement from the MG_1 side, where the orange value is the DC bus voltage, and the purple value is the current injected into the bus from MG_1. Moreover, Figure 12b depicts the contribution of MG_2, where the green value is the DC bus voltage, and the grey value is the current injected into the bus from MG_2. Furthermore, Figure 12c illustrates the measurement at the Lc point, where the contributions from MG_1 and MG_2 are shown. Table 6 summarizes Scenario 1 and its cases, listing the load demand changes alongside the power supply contributions from PV_1, BES_1, PV_2, and BES_2 sources of MG_1 and MG_2.

5.2. Scenario 2: Power Sharing during Common Load Variations

5.2.1. Case 1: Common Load Variations with Unchanged PV Supplies

This case demonstrates the effect of the microgrids on L_C variation. L_C variation occurs in two steps, where the initial load demand is 42 W. From 42 W, L_C increases to 125 W. Finally, L_C changes again from 125 W to its original demand of 42 W. For this case, other local loads, L_1 and L_2, remain the same. Moreover, throughout this case, irradiation stays unchanged, and because of that, PV_1 and PV_2 supply constant currents of 3.29 A and

2 A, respectively. Consequently, BES_1 and BES_2 are crucial in supplying the remaining load demand. At the initial condition, BES_1 and BES_2 generate 1.2 A and 1.5 A, respectively. However, when L_C promptly increases from 42 W to 152 W, BES_1 and BES_2 ramp up their generation to 3.7 A and 3 A, respectively. It is noted that BES_2 reaches its maximum limit, and BES1 supplies the rest of the demand.

Similarly, when L_C decreases from 152 W to 42 W in the final step, BES_1 and BES_2 reduce their generation to 1.2 A and 1.5 A, respectively. In this case, the capability of the microgrids to share power while common loads are changing is demonstrated. Figure 13a–c visually s the system's dynamic response, where fluctuations in the common load LC trigger adjustments in the power output from BES1 and BES2, allowing them to accommodate the varying load demands seamlessly. Figure 13a shows the experimental measurement from the MG_1 side, where orange is the DC bus voltage and purple is the current injected into the bus from MG_1. Moreover, Figure 13b depicts the contribution of MG_2, where the green value is the DC bus voltage, and the grey value is the current injected into the bus from MG_2. Furthermore, Figure 13c illustrates the measurement at the Lc point, where the contribution from MG_1, and MG_2 are shown.

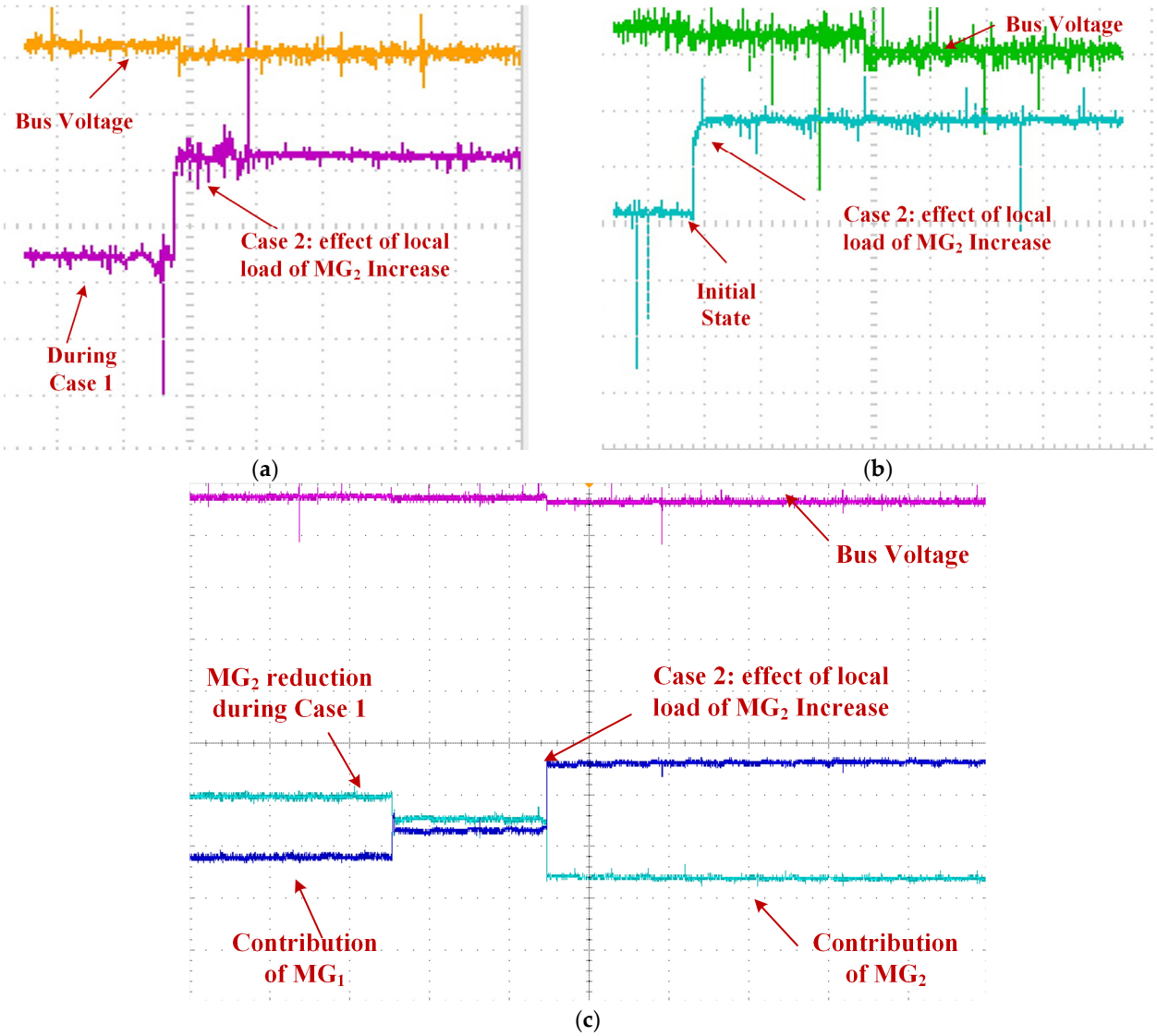

Figure 12. Behavior of each MG during Cases 1 and 2 in Scenario 1; (**a**) MG_1; (**b**) MG_2; and (**c**) shared power.

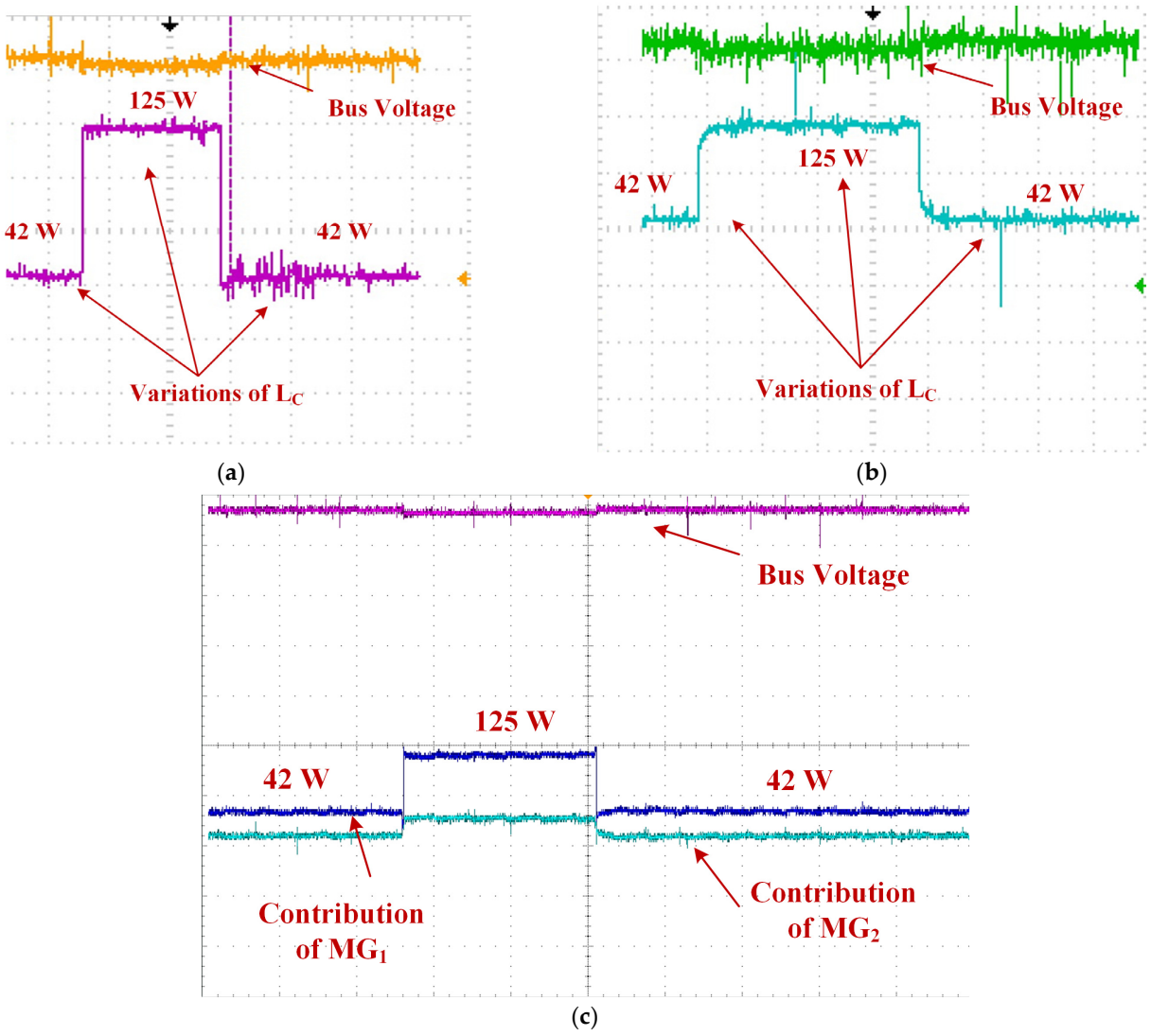

Figure 13. Behavior of each MG during Cases 1 in Scenario 2; (**a**) MG_1; (**b**) MG_2; and (**c**) shared power.

5.2.2. Case 2: Common Load Variations with Reduced PV Output in MG_2

Similar to Case 1, L_C is varied in this case. However, the steps are increased from two to four, where the initial load demand is 63 W. From 63 W, L_C reduces to 42 W. Moreover, in the next step, it further reduces to 35 W. After some period, L_C increases from 35 W to 42 W, and in the final step, to 63 W. In addition to the L_C demand changes, generation from PV2 is reduced to half throughout the period due to a 50% reduction in irradiance. However, in the case of MG_1, energy generation from PV_1 remains the same. At the same time, the energy supply from BES_2 is reduced because the battery charge becomes lower.

At the initial condition, when the demand of L_C is 63 W, BES_2 can only supply 0.4 A of power. On the other hand, PV_1 and BES_1 supply the remainder of power: 3.29 A and 2 A, respectively. In the next step, 42 W, BES_2 could not supply any power to the loads. BES1 increases its power generation from 2 A to 2.5 A to compensate for this. Moreover, in the next step, BES_1 generates more power, from 2.5 A to 3 A, to charge BES_2 while supplying L_1, L_2, and the reduced L_C. The rest of the steps are repetitions of the first step, 42 W, and the initial condition of 63 W. All these steps demonstrate the robustness of the secondary control, power-sharing ability, and stability of the interconnected microgrid.

Figure 14a–c illustrate the case, where it can be seen that the change in L_C and BES_2 charge demand triggers BES_1 to act to fulfill the load demand and BES_2 charging. Table 7 summarizes Scenario 2 and its cases, listing the load demand changes alongside the

power supply contributions from the PV_1, BES_1, PV_2, and BES_2 sources of MG_1 and MG_2. Figure 14a shows the experimental measurement from the MG_1 side, where the orange value is the DC bus voltage, and the purple value is the current injected into the bus from MG_1. Moreover, Figure 14b depicts the contribution of MG_2, where the green value is the DC bus voltage, and the grey value is the current injected into the bus from MG_2. Furthermore, Figure 14c illustrates the measurement at the Lc point, where the contributions from MG_1 and MG_2 are shown.

According to what is stated and presented in this section, the proposed EMS has proven its efficacy to cover the load demand during the uncertainties of the PV system. Further, it allows the BESS to recover during the light-load portions. This provides a concrete base for the system's expansion. As the proposed EMS relies on collecting data regarding the available capacities and loading conditions, regardless of the system components, it can be easily utilized with different microgrid configurations. In addition, the possibility of scaling it up in the real world exists. However, more computational resources for the additional system's components and prospective control signals will be needed.

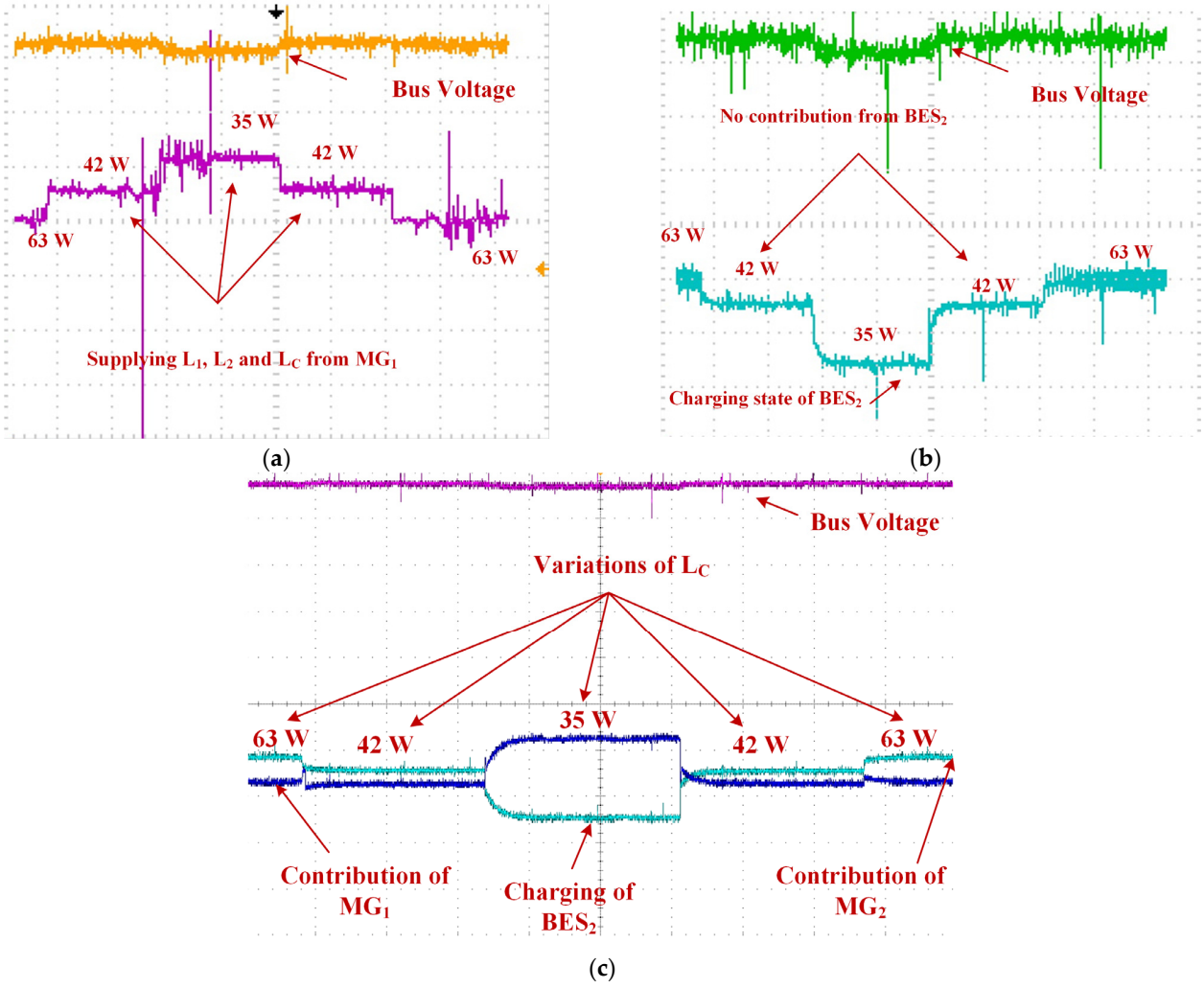

Figure 14. Behavior of each MG during Cases 2 in Scenario 2; (**a**) MG_1; (**b**) MG_2; and (**c**) shared power.

Table 7. Summary of Scenario 2 and respective experimental results.

Scenario and Cases		Scenario 02							
		Case 01				Case 02			
Load Profile (W)	L_1	125	125	125	125	125	125	125	125

Table 7. *Cont.*

Scenario and Cases		Scenario 02							
		Case 01				Case 02			
Load Profile (W)	L_2	76	76	76	76	76	76	76	76
	L_C	42	125	42	63	42	35	42	63
Total Load (W)	L_T	243	326	243	264	243	236	243	264
PV_1 Current (A)		3.29	3.29	3.29	3.29	3.29	3.29	3.29	3.29
BES_1 Current (A)		1.20	3.70	1.20	2.00	2.50	3.00	2.50	2.00
PV_2 Current (A)		2.00	2.00	2.00	1.00	1.00	1.00	1.00	1.00
BES_2 Current (A)		1.50	3.00	1.50	0.40	0.00	−1.00	0.00	0.40

6. Conclusions

A networked microgrid is an intricate system composed of multiple interconnected microgrids in close proximity, designed to enhance operational flexibility and resilience. These microgrids collaborate to avert potential power shortages within clusters by pooling renewable and energy storage resources. However, managing the diverse local resources of each microgrid presents considerable hurdles, including overseeing the charging and discharging of energy storage systems, maintaining DC bus voltage stability, and coordinating power sharing among multiple microgrids. The research encompasses the detailed hardware implementation of a two-interconnected-microgrid system within the ESRL smart-grid testbed at FIU. Each is equipped with distinct energy generation sources, battery energy storage systems (BESs), and local loads, enabling them to share power during shortages or disturbances.

Furthermore, a novel approach combining microgrid control techniques and distributed energy management is proposed to regulate shared power within the networked microgrid system effectively. The proposed energy management system has been validated through simulation and hardware implementation through several operation scenarios, witnessing uncertainties in renewable generation, sequential load variations, and relaxed portions to allow recharging of the energy storage systems. The promising results illustrate the system's ability to maintain power balance, manage renewable energy source fluctuations, and ensure reliable power supply to local and common loads within the networked microgrid system.

Author Contributions: Conceptualization, H.M.H.; methodology, H.M.H. and S.M.S.H.R.; software, H.M.H.; validation, H.M.H. and S.M.S.H.R.; formal analysis, H.M.H. and S.M.S.H.R.; investigation, H.M.H. and S.M.S.H.R.; resources, H.M.H.; data curation, H.M.H.; writing—original draft preparation, H.M.H., S.M.S.H.R. and M.S.A.; writing—review and editing, H.M.H., M.S.A. and O.A.M.; visualization, H.M.H., S.M.S.H.R. and M.S.A.; supervision, O.A.M.; project administration, O.A.M.; funding acquisition, O.A.M. All authors have read and agreed to the published version of the manuscript.

Funding: This research received no external funding.

Data Availability Statement: The original contributions presented in the study are included in the article, further inquiries can be directed to the corresponding author.

Conflicts of Interest: The authors declare no conflicts of interest.

References

1. Mirez, J. A modeling and simulation of optimized interconnection between DC microgrids with novel strategies of voltage, power and control. In Proceedings of the 2017 IEEE Second International Conference on DC Microgrids (ICDCM), Nuremburg, Germany, 27–29 June 2017; pp. 536–541.
2. Kleftakis, V.; Lagos, D.; Papadimitriou, C.; Hatziargyriou, N.D. Seamless transition between interconnected and islanded operation of DC microgrids. *IEEE Trans. Smart Grid* **2017**, *10*, 248–256. [CrossRef]

3. Han, Y.; Ning, X.; Yang, P.; Xu, L. Review of Power Sharing, Voltage Restoration and Stabilization Techniques in Hierarchical Controlled DC Microgrids. *IEEE Access* **2019**, *7*, 149202–149223. [CrossRef]
4. Hussein, H.M.; Esoofally, M.; Donekal, A.; Rafin, S.M.S.H.; Mohammed, O. Comparative Study-Based Data-Driven Models for Lithium-Ion Battery State-of-Charge Estimation. *Batteries* **2024**, *10*, 89. [CrossRef]
5. Uddin, M.; Mo, H.; Dong, D.; Elsawah, S.; Zhu, J.; Guerrero, J.M. Microgrids: A review, outstanding issues and future trends. *Energy Strategy Rev.* **2023**, *49*, 101127. [CrossRef]
6. Hussein, H.; Donekal, A.; Aghmadi, A.; Rafin, S.M.S.H.; Mohammed, O.A. State of charge estimation using data-driven models for inverter-based systems. In Proceedings of the 2023 IEEE Design Methodologies Conference (DMC), Miami, FL, USA, 24–26 September 2023; pp. 1–5.
7. Li, C.; Yang, Y.; Dragicevic, T.; Blaabjerg, F. A new perspective for relating virtual inertia with wideband oscillation of voltage in low-inertia DC microgrid. *IEEE Trans. Ind. Electron.* **2021**, *69*, 7029–7039. [CrossRef]
8. Lin, G.; Ma, J.; Li, Y.; Rehtanz, C.; Liu, J.; Wang, Z.; Wang, P.; She, F. A virtual inertia and damping control to suppress voltage oscillation in islanded DC microgrid. *IEEE Trans. Energy Convers.* **2020**, *36*, 1711–1721. [CrossRef]
9. Ullah, S.; Haidar, A.M.; Hoole, P.; Zen, H.; Ahfock, T. The current state of Distributed Renewable Generation, challenges of interconnection and opportunities for energy conversion based DC microgrids. *J. Clean. Prod.* **2020**, *273*, 122777. [CrossRef]
10. Basati, S.; Moradi, H.; Karimi, S. Voltage profile improvement in islanded DC microgrid using load shedding method based on DC bus voltage estimation. *Electr. Eng.* **2024**, 1–11. [CrossRef]
11. Zhang, H. Optimization of DC Microgrid Power and Energy Management in the Presence of Small-Scale Wind Turbine Integration and Renewable Load Shedding. *Electr. Power Compon. Syst.* **2023**, 1–15. [CrossRef]
12. Li, X.; Guo, L.; Li, Y.; Hong, C.; Zhang, Y.; Guo, Z.; Huang, D.; Wang, C. Flexible interlinking and coordinated power control of multiple DC microgrids clusters. *IEEE Trans. Sustain. Energy* **2017**, *9*, 904–915. [CrossRef]
13. Gan, L.K.; Hussain, A.; Howey, D.A.; Kim, H.-M. Limitations in energy management systems: A case study for resilient interconnected microgrids. *IEEE Trans. Smart Grid* **2018**, *10*, 5675–5685. [CrossRef]
14. Querini, P.L.; Chiotti, O.; Fernádez, E. Cooperative energy management system for networked microgrids. *Sustain. Energy Grids Netw.* **2020**, *23*, 100371. [CrossRef]
15. Naderi, M.; Khayat, Y.; Shafiee, Q.; Blaabjerg, F.; Bevrani, H. Dynamic modeling, stability analysis and control of interconnected microgrids: A review. *Appl. Energy* **2023**, *334*, 120647. [CrossRef]
16. Zaman, A.; Rahaman, H.; Reza, S.; Islam, M. Coordinated control of interconnected microgrid and energy storage system. *Int. J. Electr. Comput. Eng.* **2018**, *8*, 4781.
17. Keshta, H.E.; Malik, O.P.; Saied, E.M.; Bendary, F.M.; Ali, A.A. Energy management system for two islanded interconnected micro-grids using advanced evolutionary algorithms. *Electr. Power Syst. Res.* **2021**, *192*, 106958. [CrossRef]
18. Chen, B.; Wang, J.; Lu, X.; Chen, C.; Zhao, S. Networked microgrids for grid resilience, robustness, and efficiency: A review. *IEEE Trans. Smart Grid* **2020**, *12*, 18–32. [CrossRef]
19. Hussain, A.; Bui, V.H.; Kim, H.M. A resilient and privacy-preserving energy management strategy for networked microgrids. *IEEE Trans. Smart Grid* **2016**, *9*, 2127–2139. [CrossRef]
20. Bandeiras, F.; Pinheiro, E.; Gomes, M.; Coelho, P.; Fernandes, J. Review of the cooperation and operation of microgrid clusters. *Renew. Sustain. Energy Rev.* **2020**, *133*, 110311. [CrossRef]
21. Guan, Y.; Wei, B.; Guerrero, J.M.; Vasquez, J.C.; Gui, Y. An overview of the operation architectures and energy management system for multiple microgrid clusters. *iEnergy* **2022**, *1*, 306–314. [CrossRef]
22. Naveen, P.; Jena, P. Adaptive protection scheme for microgrid with multiple point of common couplings. *IEEE Syst. J.* **2020**, *15*, 5618–5629. [CrossRef]
23. Aazami, R.; Esmaeilbeigi, S.; Valizadeh, M.; Javadi, M.S. Novel intelligent multi-agents system for hybrid adaptive protection of micro-grid. *Sustain. Energy Grids Netw.* **2022**, *30*, 100682. [CrossRef]
24. Mehta, S.; Basak, P. A comprehensive review on control techniques for stability improvement in microgrids. *Int. Trans. Electr. Energy Syst.* **2021**, *31*, e12822. [CrossRef]
25. Ahmed, M.; Meegahapola, L.; Vahidnia, A.; Datta, M. Stability and control aspects of microgrid architectures–a comprehensive review. *IEEE Access* **2020**, *8*, 144730–144766. [CrossRef]
26. Zolfaghari, M.; Gharehpetian, G.B.; Shafie-Khah, M.; Catalão, J.P. Comprehensive review on the strategies for controlling the interconnection of AC and DC microgrids. *Int. J. Electr. Power Energy Syst.* **2022**, *136*, 107742. [CrossRef]
27. Zhou, Q.; Shahidehpour, M.; Paaso, A.; Bahramirad, S.; Alabdulwahab, A.; Abusorrah, A. Distributed control and communication strategies in networked microgrids. *IEEE Commun. Surv. Tutor.* **2020**, *22*, 2586–2633. [CrossRef]
28. Reddy, G.P.; Kumar, Y.V.P.; Chakravarthi, M.K. Communication technologies for interoperable smart microgrids in urban energy community: A broad review of the state of the art, challenges, and research perspectives. *Sensors* **2022**, *22*, 5881. [CrossRef] [PubMed]
29. Xu, Q.; Zhao, T.; Xu, Y.; Xu, Z.; Wang, P.; Blaabjerg, F. A distributed and robust energy management system for networked hybrid AC/DC microgrids. *IEEE Trans. Smart Grid* **2019**, *11*, 3496–3508. [CrossRef]

30. Aghmadi, A.; Hussein, H.; Polara, K.H.; Mohammed, O. A comprehensive review of architecture, communication, and cybersecurity in networked microgrid systems. *Inventions* **2023**, *8*, 84. [CrossRef]
31. Abhishek, A.; Ranjan, A.; Devassy, S.; Verma, B.K.; Ram, S.K.; Dhakar, A.K. Review of hierarchical control strategies for DC microgrid. *IET Renew. Power Gener.* **2020**, *14*, 1631–1640. [CrossRef]
32. Olivares, D.E.; Canizares, C.A.; Kazerani, M. A centralized energy management system for isolated microgrids. *IEEE Trans. Smart Grid* **2014**, *5*, 1864–1875. [CrossRef]
33. Islam, M.; Yang, F.; Amin, M. Control and optimisation of networked microgrids: A review. *IET Renew. Power Gener.* **2021**, *15*, 1133–1148. [CrossRef]
34. Liu, G.; Ollis, T.B.; Ferrari, M.F.; Sundararajan, A.; Chen, Y. Distributed Energy Management for Networked Microgrids Embedded Modern Distribution System Using ADMM Algorithm. *IEEE Access* **2023**, *11*, 102589–102604. [CrossRef]
35. Bazmohammadi, N.; Tahsiri, A.; Anvari-Moghaddam, A.; Guerrero, J.M. A hierarchical energy management strategy for interconnected microgrids considering uncertainty. *Int. J. Electr. Power Energy Syst.* **2019**, *109*, 597–608. [CrossRef]
36. Hussein, H.; Aghmadi, A.; Nguyen, T.L.; Mohammed, O. Hardware-in-the-loop implementation of a Battery System Charging/Discharging in Islanded DC Micro-grid. In Proceedings of the SoutheastCon 2022, Mobile, AL, USA, 26 March–3 April 2022; pp. 496–500.
37. Hussein, H.; Aghmadi, A.; Mohammed, O.A. Design and Analysis of Voltage Control for Islanded DC Microgrids Based on a Fuzzy-PI Controller. In Proceedings of the 2023 IEEE Green Technologies Conference (GreenTech), Denver, CO, USA, 19–21 April 2023; pp. 229–233.
38. Sinha, S.; Ghosh, S.; Bajpai, P. Power sharing through interlinking converters in adaptive droop controlled multiple microgrid system. *Int. J. Electr. Power Energy Syst.* **2021**, *128*, 106649. [CrossRef]
39. Hu, J.; Shan, Y.; Guerrero, J.M.; Ioinovici, A.; Chan, K.W.; Rodriguez, J. Model predictive control of microgrids—An overview. *Renew. Sustain. Energy Rev.* **2021**, *136*, 110422. [CrossRef]
40. Han, Y.; Zhang, K.; Li, H.; Coelho, E.A.A.; Guerrero, J.M. MAS-based distributed coordinated control and optimization in microgrid and microgrid clusters: A comprehensive overview. *IEEE Trans. Power Electron.* **2017**, *33*, 6488–6508. [CrossRef]
41. Simpson-Porco, J.W.; Shafiee, Q.; Dorfler, F.; Vasquez, J.C.; Guerrero, J.M.; Bullo, F. Secondary frequency and voltage control of islanded microgrids via distributed averaging. *IEEE Trans. Ind. Electron.* **2015**, *62*, 7025–7038. [CrossRef]
42. Tazi, K.; Abbou, F.M.; Abdi, F. Multi-agent system for microgrids: Design, optimization and performance. *Artif. Intell. Rev.* **2020**, *53*, 1233–1292. [CrossRef]
43. Kong, X.; Liu, D.; Xiao, J.; Wang, C. A multi-agent optimal bidding strategy in microgrids based on artificial immune system. *Energy* **2019**, *189*, 116154. [CrossRef]
44. Abdelrahman, M.S.; Hussein, H.; Mohammed, O.A. Rule-based power and energy management system for shipboard microgrid with HESS to mitigate propulsion and pulsed load fluctuations. In Proceedings of the 2023 IEEE Green Technologies Conference (GreenTech), Denver, CO, USA, 19–21 April 2023; pp. 224–228.
45. Poudel, B.P.; Mustafa, A.; Bidram, A.; Modares, H. Detection and mitigation of cyber-threats in the DC microgrid distributed control system. *Int. J. Electr. Power Energy Syst.* **2020**, *120*, 105968. [CrossRef]
46. Sahoo, S.; Dragičević, T.; Blaabjerg, F. Multilayer resilience paradigm against cyber attacks in DC microgrids. *IEEE Trans. Power Electron.* **2020**, *36*, 2522–2532. [CrossRef]
47. Alnowibet, K.; Annuk, A.; Dampage, U.; Mohamed, M.A. Effective energy management via false data detection scheme for the interconnected smart energy hub–microgrid system under stochastic framework. *Sustainability* **2021**, *13*, 11836. [CrossRef]
48. Tan, S.; Xie, P.; Guerrero, J.M.; Vasquez, J.C. False data injection cyber-attacks detection for multiple DC microgrid clusters. *Appl. Energy* **2022**, *310*, 118425. [CrossRef]
49. Boyd, M.T.; Klein, S.A.; Reindl, D.T.; Dougherty, B.P. Evaluation and Validation of Equivalent Circuit Photovoltaic Solar Cell Performance Models. *J. Sol. Energy Eng.-Trans. ASME* **2011**, *133*, 021005. [CrossRef]
50. Hussein, H.; Aghmadi, A.; Abdelrahman, M.S.; Rafin, S.M.S.H.; Mohammed, O. A review of battery state of charge estimation and management systems: Models and future prospective. *Wiley Interdiscip. Rev. Energy Environ.* **2024**, *13*, e507. [CrossRef]
51. Rafin, S.S.H.; Hussein, H.; Mohammed, O.A. An Introduction to Power Electronics Design Methodology. In Proceedings of the 2023 IEEE Design Methodologies Conference (DMC), Miami, FL, USA, 24–26 September 2023; pp. 1–6.
52. Saleh, M.; Esa, Y.; Mhandi, Y.; Brandauer, W.; Mohamed, A. Design and implementation of CCNY DC microgrid testbed. In Proceedings of the 2016 IEEE Industry Applications Society Annual Meeting, Portland, OR, USA, 2–6 October 2016; pp. 1–7. [CrossRef]
53. Abdelrahman, M.S.; Kharchouf, I.; Nguyen, T.L.; Mohammed, O.A. A Hybrid Physical Co-Simulation Smart Grid Testbed for Testing and Impact Analysis of Cyber-Attacks on Power Systems: Framework and Attack Scenarios. *Energies* **2023**, *16*, 7771. [CrossRef]
54. Chalh, A.; Motahhir, S.; El Hammoumi, A.; El Ghzizal, A.; Derouich, A. Study of a low-cost PV emulator for testing MPPT algorithm under fast irradiation and temperature change. *Technol. Econ. Smart Grids Sustain. Energy* **2018**, *3*, 11. [CrossRef]
55. Choi, S.; Park, S.; Hong, J.; Won, J. A Design and Validation of 400 W PV Emulator Using Simple Equivalent Circuit for PV Power System Test. *Energies* **2023**, *16*, 1561. [CrossRef]

56. Bandyopadhyay, S.; Qin, Z.; Ramirez-Elizondo, L.; Bauer, P. Comparison of Battery Technologies for DC Microgrids with Integrated PV. In Proceedings of the 2019 IEEE International Conference on DC Microgrids (ICDCM), Matsue, Japan, 20–23 May 2019; pp. 1–9.
57. Zakeri, B.; Syri, S. Electrical energy storage systems: A comparative life cycle cost analysis. *Renew. Sustain. Energy Rev.* **2015**, *42*, 569–596. [CrossRef]